A WIND MODEL FOR AN ELEVATED STOL-PORT CONFIGURATION

by J. A. Peterka and J. E. Cermak

1. Report No. NASA CR-2450	2. Government Accession No.	3. Recipient's Catalog No.
4. Title and Subtitle A Wind Model for An Elevated STOL-Port Configuration		5. Report Date JULY 1974
		6. Performing Organization Code
7. Author(s) J. A. Peterka and J. E. Cermak		8. Performing Organization Report No.
		10. Work Unit No.
9. Performing Organization Name and Address Colorado State University Fluid Mechanics Program Fluid Dynamics and Diffusion Laboratory Department of Civil Engineering Fort Collins, Colorado		
		11. Contract or Grant No. NAS 2-7396
		13. Type of Report and Period Covered
12. Sponsoring Agency Name and Address National Aeronautics and Space Administration Washington, D.C. 20546		Contractor Report/Final
		14. Sponsoring Agency Code

15. Supplementary Notes

16. Abstract

Measurements of mean velocity magnitude and direction as well as three-dimensional turbulence intensity were made in the flow over a model of an elevated STOL-port. A 1:300 scale model was placed in a wind tunnel flow simulating the mean velocity profile and turbulence characteristics of atmospheric winds over a typical city environment excluding detailed wake structures of possible nearby buildings. Hot-wire anemometer measurements of velocity and turbulence were made along approach and departure paths of aircraft operating on the runway centerline and at specified lateral distances from the centerline. Approach flow directions simulated were 0 and 30 degrees to the runway centerline.

17. Key Words (Suggested by Author(s)) Elevated STOL-port Wind model Turbulence	18. Distribution Statement UNCLASSIFIED-UNLIMITED CAT. 11		
19. Security Classif. (of this report) UNCLASSIFIED	20. Security Classif. (of this page) UNCLASSIFIED	21. No. of Pages 39	22. Price* $3.25

ABSTRACT

Measurements of mean velocity magnitude and direction as well as three-dimensional turbulence intensity were made in the flow over a model of an elevated STOL-port. A 1:300 scale model was placed in a wind tunnel flow simulating the mean velocity profile and turbulence characteristics of atmospheric winds over a typical city environment excluding detailed wake structures of possible nearby buildings. Hot-wire anemometer measurements of velocity and turbulence were made along approach and departure paths of aircraft operating on the runway centerline and at specified lateral distances from the centerline. Approach flow directions simulated were 0 and 30 degrees to the runway centerline.

ACKNOWLEDGMENTS

TABLE OF CONTENTS

LIST OF TABLES

LIST OF FIGURES

LIST OF SYMBOLS

Symbol	Definition
X	coordinate axis parallel to STOL port centerline, positive upwind, zero at downwind edge of structure
Y	horizontal coordinate with zero on center data plane
Z	vertical coordinate, positive downward, zero on the top surface of the STOL port
U	mean velocity in X direction
V	mean velocity in Y direction
W	mean velocity in Z direction
U_{vector}	mean velocity vector magnitude
U_∞	value of U_{vector} above the boundary layer
u	fluctuating velocity in X direction
v	fluctuating velocity in Y direction
w	fluctuating velocity in Z direction
U_T	flow calibrator velocity
α	horizontal angle of U_{vector} in X, Y, Z coordinate system
β	vertical angle of U_{vector} in X, Y, Z coordinate system
θ	flow calibrator angle of incidence
A,B,C $\alpha_1, \alpha_2, \alpha_3$	calibration constants
E	mean voltage

1. INTRODUCTION

With the serious consideration of STOL aircraft as a major transportation
mode, extensive investigations of STOL feasibility have been and are underway.
One of the important factors in STOL-port design recognized by the FAA [1] is
the effect of winds on aircraft operating from these facilities. Interest in
this problem has accelerated in the last few years as evidenced by an
increased level of investigation. The effects of atmospheric turbulence on
small aircraft performance has been discussed [2]. Cass et al. [3]
investigated the characteristics of turbulence about an airport site and
found agreement on the influence of nearby buildings with a study by Colmer
[4] of the wake structure behind an isolated hangar. Kurlowski et al. [5]
have presented an improved turbulence model for use in flight simulations.

One STOL-port configuration under study is an elevated structure. It
would have the advantage of getting an aircraft up away rapidly from
turbulence associated with surrounding structures. One potential problem for
this type of STOL-port is the influence of the structure itself on the winds
in the regions through which the aircraft must fly. A preliminary, qualitative
evaluation of STOL-port design was performed by Parker et al. [6] which showed
that proper design could substantially alleviate structure induced flow
problems. The purpose of the present study was to determine quantitatively
the influence of a proposed elevated STOL-port on the mean flow and turbulence
over the structure. The results of this study are to be incorporated into a
piloted-simulator to determine the effect on pilot-vehicle performance.

The study was performed by placing a model of the proposed elevated
STOL-port in a wind tunnel specifically designed to simulate atmospheric winds.
Proper modeling of the atmospheric boundary layer flow approaching the model

is essential in providing accurate determination of the flow characteristics. Modeling criteria are discussed in Reference 7. Mean velocity and three-dimensional turbulence measurements were made along typical approach and departure paths for STOL aircraft. Two wind directions were employed: one parallel to the flight path and one 30 degrees to the flight path. Measurements without the model in place allowed the influence of the structure to be evaluated.

2. EXPERIMENTAL CONFIGURATION

2.1 Wind Tunnel

The wind study was performed in the Environmental Wind Tunnel located in the Fluid Dynamics and Diffusion Laboratory at Colorado State University, Fig. 1. The tunnel is an open circuit facility driven by a variable pitch propeller. The test section is nominally 12 ft (3.66 m) wide, 8 ft (2.44 m) high, and 52 ft (15.8 m) long. The roof is adjustable to maintain a zero pressure gradient along the test section. The mean velocity can be adjusted continuously from 2 to 24 fps (0.61 to 7.31 mps) with the 10 hp motor and to a maximum velocity of 60 fps (18.3 mps) with the 150 hp motor.

2.2 Model

The elevated STOL-port structure has dimensions of 2200 ft (670.5 m) by 1200 ft (365.8 m) by 100 ft (30.5 m) high. In order to provide maximum resolution in the data, the largest scale model feasible within the physical limitations imposed by the wind tunnel was chosen. Scale selected was 1:300. Dimensions of the scaled model were 88 in (2.23 m) long, 48 in (1.22 m) wide, and 4 in (10.2 cm) high. The model was placed 25 ft (7.6 m) from the test section entrance on a turntable to allow ease of rotation. The turbulent boundary layer approaching the structure was developed with a carefully designed trip at the test section entrance 12 in (30.5 cm) high consisting of 2.5 in (6.4 cm) diameter tubes followed by ½ in (1.27 cm) gravel uniformly spread over the floor. A photograph of the model in-place in the wind tunnel is shown in Fig. 2.

No attempt was made to simulate the detailed wake of individual structures in the flow approaching the model. Instead, a turbulent boundary layer was generated whose characteristics simulated a typical atmospheric boundary-layer flow over an urban environment.

3. INSTRUMENTATION AND DATA ACQUISITION

3.1 Flow Visualization

Visualization of the flow over the model is helpful in understanding and interpreting mean and fluctuating pressures, in defining zones of separated and reattached flow, and in identifying size and intensity of vortices generated by building corners. Titanium tetrachloride smoke was released from sources on and near the model and photographic records were made of the flow. Conclusions based on these observations are discussed in section 4.1.

3.2 Mean Velocity and Flow Direction

To measure three components of mean flow and the mean velocity direction a new hot-wire anemometer measurement scheme which has been under development at the Fluid Dynamics and Diffusion Laboratory at Colorado State University was employed. The procedure utilized a conventional 45 degree yawed hot-wire sensing element 0.00015 in. (0.0038 mm) in diameter with an active length of 0.050 in. (1.25 mm). A Colorado State University hot-wire anemometer unit was used with the sensing element. The unit is characterized by good stability and high signal to noise ratio. A photograph of the probe is shown in Fig. 3.

Operation of the measurement system required that the hot-wire be calibrated for flow speed and angle-of-flow incidence to the wire. A Thermo-Systems flow calibrator was used with a Colorado State University built probe positioner. The calibration data was fit to a modified King's law equation of the form

$$E^2 = A + BU_T^C \, f(\theta)$$

$$f(\theta) = 1 + \alpha_1\theta + \alpha_2\theta^2 + \alpha_3\theta^3$$

(1)

where U_T and θ are the velocity and angle to the wire (0 degrees was parallel to the wire) of the calibration flow, E is the mean voltage output from the anemometer, and A, B, C, α_1, α_2, α_3 are calibration constants used to fit the equation to the data. Thirty calibration points representing 5 velocities at 6 angles were used in a computer program to fit the calibration-equation coefficients by least squares. Calculations were performed on the Colorado State University CDC6400 computer. A typical calibration is shown in Fig. 4.

To obtain mean velocity data, the probe was mounted in the wind tunnel approximately 20 degrees to the horizontal plane and 20 degrees to the tunnel vertical centerline plane. Twelve to 15 mean voltages at different rotational positions were obtained using an integrating digital voltmeter for 30 seconds. This positioned the sensing element at angles to the mean flow ranging from about 20° to 70°. Data was reduced by finding the three mean velocity components U_m , V_m, W_m which provided the least squares fit of the data to Eq. 1 in a coordinate system aligned with the probe axis of rotation. Because the equation cannot be solved explicitly for the velocity components, an iteration method was devised to converge to the correct solution from initial velocity estimates. Convergence was obtained in 6 to 8 interations with simple initial estimates. A vector rotation was applied to the velocity components to transform them from the probe oriented coordinate system into the coordinate system defined for the STOL-port (Section 3.4 and Figure 5).

Horizontal and vertical flow angles were computed from the velocity components. All calculations were performed on the Colorado State University CDC6400 computer.

The probe attitude relative to the wind tunnel coordinate system was set with an optical alignment system. A laser light source was aligned along the data plane being measured. A mirror mounted to the probe support reflected the light back to a target placed near the laser. Using this system, the probe could be aligned to a predetermined attitude within 0.2 degrees.

The accuracy of the mean velocity measurements was measured in such a way that the error included both the variablity inherent in the wind-tunnel flow and the uncertainty due to the measurement probe itself. The analysis was performed by measuring several vertical pro-files in the wind tunnel with the model removed but the roughness remaining. The total error was the difference between the assumed zero angle of flow and the angle measured with the probe. The standard deviation in α (the flow angle in the horizontal plane) was 0.90 degrees while the standard deviation in β (the flow angle in the vertical plane) was 0.79 degrees. These figures compare favorably to the angular resolution of 5.0 degrees in the horizontal and 1.0 degrees in the vertical requested in the statement of work defining the scope of this investigation. The error in the magnitude of the total velocity vector was not measured precisely because the errors in the comparative pitot tube measurements appeared from tests to be larger than those of the probe itself. The error appeared to be one percent or less.

3.3 Turbulence Intensities

Measurement of turbulence intensity was made with a standard X-wire probe. The probe was aligned to the mean flow direction determined previously with the optical alignment system described above. Each of the wires was calibrated individually with the Thermo-Systems calibrator. Data reduction used the procedure described by Klatt [12] which accounts for differences in wire calibration for each wire. The turbulence quantities calculated were u_{rms}/U_{vector}, v_{rms}/U_{vector}, and w_{rms}/U_{vector} where u, v, and w are the three fluctuating velocities in directions X, Y, Z and U_{vector} is the local mean velocity magnitude.

An independent check of the crossed-wire turbulence results was made by measuring at several data locations the longitudinal component of velocity fluctuation with a hot-wire placed normal to the flow. The results of the comparative measurements are shown by the triangles and squares in Fig. 5. The results are in excellent agreement.

3.4 Data Locations

Except for vertical profiles to determine the characteristics of the approach flow, all data was taken along data lines lying within data planes. Two data planes were used: 1) Center Data Plane, a vertical plane through the center of the building 600 ft (182.0 m) from either side and 2) Side Data Plane, a plane parallel to the Center Plane but 150 ft (45.7 m) in from one side. These data planes provided information on the conditions an aircraft could experience during take-off or landing at the center of the runway and near the edge of the structure.

A data line was established in each data plane along lines expected to be used for approach, runway, and departure. The approach

segment was defined as a line extending upward at a 7.5 degree angle
to the horizontal in a downwind direction from a point on the runway
centerline 350 ft (106.7 m) from the downwind edge of the roof. The
departure segment was defined as a line extending upwards at a 7.5
degree angle to the horizontal in an upwind direction from a point on
the runway centerline 1000 ft (304.8 m) from the downwind edge of the
roof. The runway segment was defined as a line 15 ft (4.6 m) above
the runway centerline that connected the approach segment to the
departure segment. The data lines are shown in Fig. 6.

Data points were located along the data lines to provide adequate
resolution of the measurements. Five data points were evenly spaced
along the runway segment, seven points were located along the approach
segment and thirteen points were located along the departure segment for
a total of twenty-five data points per data line.

A coordinate system fixed to the STOL-port was defined for data
reporting purposes (Fig. 6). Y = 0 defined the particular data plane
of interest. Negative Z represented height above the STOL-port roof
while positive X was distance into the wind from the downwind edge of
the roof. This coordinate system is the same as provided in the statement
of work defining the scope of this investigation.

4. RESULTS

4.1 Flow Visualization

Structures with sharp corners placed in an atmospheric flow are
known to generate vortices from leading corners when the wind is at
an angle to a building side. Increased turbulence in the approach flow
tends to break down organized vortex structures more rapidly. A primary
objective of the visualization was to identfy this vortex structure by
observing its strength and coherence downstream. Smoke flow showed
significant vorticity with an axis parallel to the structure's long side
over the model near the windward side for flow approaching at 30 degrees
to the building long axis. This vorticity emanated from the leading
corner but was fed along its length by separation of flow along the
leading edge of the roof. Flow reattached to the roof not far downstream
from the leading edge, but neither the separation streamline nor
reattachment region were well defined. Diffusion of smoke occurred so
rapidly in the turbulence that the above described phenomena could
not be adequately captured on film. The influence of this vorticity
on flight patterns should be confined to the windward side data plane
for the 30 degree wind.

Lifting of the flow approaching the structure appeared to extend to
rather high elevations over the building. A variation in vertical flow
angle of possible significance to aircraft was observed with the smoke
for all cases in the region over the structure's leading edge. All
conclusions obtained from flow visualization were confirmed with the
velocity measurements reported in sections 4.3 and 4.4.

4.2 Data Scaling

Velocity data was taken for a reference velocity outside the
boundary layer of 23.2 fps (7.07 mps). This provided a wind tunnel

Reynolds number ($\frac{UD}{\nu}$) based on building height and approach velocity

at that height of 3 x 10^4. This is the smallest of the Reynolds

numbers which can be calculated using building geometry for the length

scale, and a characteristic approach velocity. At this value of

Reynolds number, the flow structure should be Reynolds number indepen-

dent; that is a component of mean velocity at any point in the flow

normalized by the velocity U_∞ at the edge of the boundary layer should

be independent of the approach velocity U_∞. In addition, a turbulence

intensity as defined in section 3.3 at any point in the flow should

be independent of U_∞. Thus the data taken at 23.2 fps (7.07 mps) can

be used to obtain mean and root-mean-square velocities for any desired

approach velocity. Mean velocity magnitudes are obtained by simply

multiplying the nondimensional velocities (i.e. U/U_∞) by the desired

free stream velocity. Root-mean-square velocities must, in addition,

be mutiplied by the nondimensionalized local mean velocity,

$\frac{U_{vector}}{U_\infty}$, since the turbulence quantities were made nondimensional

with the local velocity according to standard practice.

An experimental verification of the Reynolds number independence

was performed by remeasuring several quantities at a different approach

velocity. A comparison of mean velocity profiles taken along the upwind

centerline data line for a 30 degree approach wind for 23.2 fps (7.07

mps) and 15 fps (4.57 mps) is shown in Fig. 7. The comparison is good.

The profile shown should be valid for all approach velocities above

15 fps. A comparison of longitudinal turbulence intensity for a portion

of the same data line for identical velocities is shown by the circles

and triangles in Fig. 5. The agreement is within the accuracy required

for the study. The turbulent intensities are thus valid for the same

range of approach velocities as the mean velocity.

4.3 Mean Velocities

Mean velocity profiles were obtained at the model site with the
building removed to provide a baseline for comparison of data with the
model in place. These profiles are shown in Figs. 8 and 9. The
vertical coordinate shown, $-\frac{(Z-H)}{\delta}$, is in the coordinate system
defined in Section 3.4 and represents the nondimensional distance
above the ground level. The velocities are shown in both logarithmic
and semi-logarithmic form to demonstrate the characteristics of the
boundary layer. For the logarithmic description, the velocity profile
is expressed in the following form:

$$\frac{U}{U_\infty} = (-\frac{Z-H}{\delta})^{0.345}$$

The exponent 0.345 is centered within the range of values expected for
a city environment. The velocity profile in semi-logarithmic form
shows a linear profile as is expected for a neutrally stable atmospheric
boundary layer. The roughness length Z_o is 7.2 ft. (2.2 m) in the
full scale, a very reasonable value for a city roughness.

Mean velocity magnitudes and directions with the model in place
are recorded in Tables 1 and 2. Table 1 shows the magnitude of the
mean velocity vector and its horizontal and vertical angles to the
reference coordinate system for each data point in the 5 data planes of
interest. The velocity vector magnitude is recorded as U_{vector}/U_∞
where U_∞ is the velocity at the edge of the boundary layer. Definitions
of the horizontal angle α and vertical angle β are given in Fig. 10.
With the model oriented so that the wind vector is from an angle to the
left for a landing or departing aircraft, an α more positive than the
prevailing wind angle would indicate a local wind to the right of the

prevailing direction. A positive β angle indicates an upward vertical component in the wind vector. The data planes investigated were the center and one side plane for a zero degree approach wind and the center and both side planes for a 30 degree wind approaching from the left. Table 1 also shows the magnitude of the mean velocity vector on the center data plane at zero degree wind azimuth with the STOL port removed from the wind tunnel. The α and β angles were nominally zero for that case.

A breakdown for the velocity vector into components is shown in Table 2. Data is supplied only for the 30 degree case since the V and W components were negligibly small for the 0 degree cases.

An overall view of the mean flow characteristics along the data lines is shown in Fig. 11. The individual arrows represent the magnitude and horizontal direction of the mean flow measured at the arrow base on three data lines. The strongest effects are seen in the upwind side data plane. The effect of the model on the velocity magnitude can be seen in Fig. 12. The three curves represent (1) the approach flow without the model and (2) with the model, the velocities on the approach and departure segments of the center data line for a zero degree wind. Reduction in wind velocity with the model in place is evident for both cases.

Of great concern to aircraft is the angle of the flow over the structure -- in particular, rapid changes in vertical angle of flow may cause difficulties for small aircraft. Plots of vertical and horizontal angles for the mean flow vector are plotted in Figs. 13 through 16. Figure 13 shows the vertical angle for the data lines in the center and side planes for a zero degree wind. Extremum in angle

occur at or just off the edge of the structure with little change in angle over the center portion of the structure. Figure 14 shows the horizontal flow angle for the same conditions as the previous figure. No sharp gradients exist in the angles. The approximately one degree bias in the center plane data is due to a small cross flow tendency in the lower third of the 8 ft (2.44 m) height of the wind tunnel flow (the model was aligned precisely with the geometrical wind tunnel axis).

The vertical flow angle for the center plane and both side planes is shown in Fig. 15. All three show the same qualitative features with the magnitude of effect differing slightly. Again, the largest gradient in angle occurred near the edges of the model. Figure 16 shows the horizontal angle for the same conditions. The gradient of angle is severe only for the windward side plane, an effect also noted in Fig. 11. Smoke flow observations tended to show the same effect.

4.4 Turbulence Intensities

Longitudinal turbulence intensity at the building site without the model in place is shown in Fig. 17 as a function of height above the surface. The data provides a comparison for data taken with the model in place.

Turbulence intensities in the three directions defined by the coordinate system defined in Section 3.4 are listed in Table 3. Measurement positions for two data planes at a 0 degree wind and three data planes at 30 degree wind were the same as for mean velocities. Some characteristics of the turbulent field can be seen from Figs. 18 and 19. For a 0 degree wind, the longitudinal fluctuations varied

smoothly reaching a maximum amplitude of 15 to 17 percent in the two data planes at about 80 to 100 ft above the STOL port surface on the departure line. The fluctuations varied more for the 30 degree wind (Fig. 19) reaching a maximum value of 23 percent near the takeoff point on the departure line on the windward data plane. Maximum value on the other two planes at 30° were 12 percent. The spatial variability of the windward data was confirmed with repeat measurements. The turbulence components in the Y and Z directions generally followed the same trends as the longitudinal component, but at lower amplitudes.

5. CONCLUSIONS

Measurements of mean velocity magnitude and direction as well as three-dimensional turbulence intensity were made in the flow over a modeled STOL port. The flow approaching the model was representative of flow over a city environment excluding detailed wake structures of possible nearby buildings. The measurements were made along approach and departure paths of aircraft operating on the building center line and 150 ft in from each side of the structure with wind directions parallel and 30 degrees to the flight path. Results of the measurements showed the worst environment of those studied to be the flight path nearest the windward side of the STOL-port with a 30 degree wind. Sizable turbulence intensities and gradients of mean flow angle were found, however, even for the centerline with a 0 degree wind.

The present study did not attempt to modify the flow characteristics over the structure with vortex spoiling devices. Relatively simple modifications to the local geometry at the building edge which would not interfere with aircraft safety should help to alleviate some of the adverse flow characteristics seen in this study. Since the elevated STOL port was conceived for use near a large city, the wakes of other structures in the vicinity may cause larger effects on the flow than the structure itself. For this reason, additional wind-tunnel tests with realistic city surroundings should be undertaken before suitability of the elevated STOL port concept is accepted.

REFERENCES

1. *Planning and Design Criteria for Metropolitan STOL Ports,* Federal Aviation Administration, Washington, D.C., Nov. 1970.

2. Burnham, J. and F. O'Hara, "The Atmospheric Environment and Aircraft — Now and the Future," TM AERO 1067, Royal Aircraft Establishment, Farnborough Hants, England, July 1968.

3. Cass, Stanley D., J. R. Scoggins, and H. L. Chevalier, "Low-Altitude Atmospheric Turbulence around an Airport," Jl. Aircraft, Vol. 10, pp. 157-163, March 1973.

4. Colmer, M., "Some Full-Scale Measurements of the Flow in the Wake of a Hangar," Aeronautical Research Council Current Papers No. 1166, Ministry of Aviation Supply, Her Majesty's Stationery Office, London, England, 1971.

5. Kurkowski, R. L., G. H. Fichtl, and J. Gera, "Development of Turbulence and Wind Shear Models for Simulator Application," NASA Aircraft Safety and Operating Problems, Vol. 1, NASA Langley Research Center, Hampton, Virginia, pp. 291-306, May 1971.

6. Parker, H. M., J. N. Blanton, and K. J. Grunwald, "Some Aspects of the Aerodynamics of STOL Ports," NASA Aircraft Safety and Operating Problems, Vol. 1, NASA Langley Research Center, Hampton, Virginia, pp. 263-276, May 1971.

7. Cermak, J. E., "Laboratory Simulation of the Atmospheric Boundary Layer," AIAA Jl., Vol. 9, pp. 1746-1754, Sept. 1971.

8. Klatt, F., "The X Hot-Wire Probe in a Plane Flow Field," DISA Information, No. 8, DISA Elektronik, Herler, Denmark, July 1969.

TABLE 1

NORMALIZED MEAN VELOCITIES AND ANGLES
(U_∞ = 23.2 ft/sec)

X(ft)	-z(ft)	WITHOUT MODEL $\frac{U_{vector}}{U_\infty}$	WIND AT 0 DEGREES CENTER DATA PLANE			WIND AT 0 DEGREES SIDE DATA PLANE			WIND AT 30 DEGREES LEE SIDE DATA PLANE			WIND AT 30 DEGREES CENTER DATA PLANE			WIND AT 30 DEGREES WINDWARD SIDE DATA PLANE		
			$\frac{U_{vector}}{U_\infty}$	α (Deg)	β (Deg)	U_{vector}	α (Deg)	β (Deg)	$\frac{U_{vector}}{U_\infty}$	α (Deg)	β (Deg)	$\frac{U_{vector}}{U_\infty}$	α (Deg)	β (Deg)	$\frac{U_{vector}}{U_\infty}$	α (Deg)	β (Deg)
-750	175	0.90	0.90	1.2	-2.5	0.85	.5	-2.2	0.78	-30.1	-3.0	0.79	-32.3	-3.7	0.76	-32.7	-1.4
-300	100	0.81	0.80	0.7	-2.3	0.77	-0.8	-3.5	0.75	-29.1	-2.6	0.74	-30.5	-3.7	0.73	-34.0	-0.1
-150	81	0.79	0.72	0.9	-1.8	0.76	0.9	-1.8	0.71	-29.5	-2.5	0.73	-29.2	-2.9	0.75	-34.0	0.6
-50	68	0.77	0.71	0.9	-.8	0.73	-0.5	-1.8	0.70	-28.9	-1.4	0.69	-29.3	-1.7	0.68	-35.7	0.7
+50	54	0.74	0.67	0.7	-.1	0.69	-0.7	-0.2	0.68	-29.3	-0.3	0.64	-28.7	-1.1	0.63	-35.7	-0.2
150	41	0.71	0.64	1.3	.5	0.66	-0.6	0.6	0.67	-29.5	-0.3	0.59	-28.9	0.4	0.58	-30.1	1.6
250	28	0.69	0.60	1.1	1.6	0.60	-0.1	1.4	0.65	-29.9	0.0	0.56	-28.0	0.3	0.52	-29.9	0.9
350	15	0.65	0.56	1.5	1.4	0.56	-0.3	-0.2	0.61	-30.3	1.1	0.53	-27.1	0.4	0.49	-23.1	1.6
512	15	0.65	0.54	1.0	1.4	0.53	-0.6	1.0	0.63	-30.8	0.4	0.52	-28.5	0.5	0.47	-25.4	2.3
675	15	0.65	0.54	2.0	1.5	0.55	0.0	0.9	0.64	-32.2	0.0	0.52	-29.3	1.2	0.45	-25.8	1.8
938	15	0.65	0.52	1.3	1.5	0.53	0.2	1.3	0.62	-33.0	0.9	0.51	-28.8	1.1	0.44	-24.2	1.8
1000	15	0.65	0.51	1.9	1.3	0.53	-0.1	0.5	0.54	-34.3	1.1	0.57	-30.2	1.0	0.45	-25.9	2.0
1100	28	0.69	0.52	1.2	1.5	0.58	0.5	1.0	0.55	-33.9	1.5	0.62	-30.9	0.9	0.47	-30.6	1.3
1200	41	0.71	0.54	0.7	1.3	0.59	0.4	1.3	0.57	-34.0	0.8	0.66	-30.6	0.8	0.52	-35.1	1.3
1300	54	0.74	0.57	1.2	1.3	0.61	0.0	0.7				0.70	-31.4	0.5	0.57	-38.1	0.8
1400	68	0.77	0.62	0.7	1.3	0.62	0.5	2.4	0.63	-33.0	0.3	0.71	-31.5	0.6	0.60	-36.0	0.7
1500	81	0.79	0.64	1.0	1.2	0.68	0.3	0.5	0.64	-32.3	0.1	0.71	-30.8	0.8	0.63	-34.5	1.0
1600	94	0.81	0.70	0.4	.3	0.69	0.0	0.0	0.67	-31.5	0.2	0.73	-30.6	1.0	0.70	-33.6	0.0
1700	107	0.83	0.73	0.8	.7	0.75	1.0	0.0	0.71	-31.1	-0.5	0.70	-29.9	1.7	0.75	-33.5	0.3
1875	130	0.87	0.80	1.0	.7	0.80	1.7	0.5	0.77	-30.0	-0.1	0.70	-29.5	1.9	0.81	-30.6	0.4
2050	153	0.89	0.87	0.9	1.9	0.85	2.1	1.8	0.81	-28.8	2.0	0.82	-28.0	2.6	0.87	-29.2	0.6
2200	174	0.91	0.89	1.3	4.2	0.86	2.1	4.1	0.85	-29.5	3.8	0.85	-28.3	4.0	0.88	-28.7	1.6
2350	194	0.86	0.89	1.4	3.5	0.85	2.4	3.6	0.84	-29.6	2.8	0.87	-29.3	3.8	0.87	-28.9	1.5
2650	233	0.93	0.96	1.8	1.57	0.87	2.7	1.41	0.84	-27.9	1.5	0.86	-27.2	0.9	0.85	-28.5	2.3
2950	272	1.0	0.99	2.0	.43	0.91	2.7	.71	0.89	-27.3	-0.2	0.87	-27.4	0.8	0.90	-27.4	1.6

TABLE 2

MEAN VELOCITY COMPONENTS FOR 30 DEGREE WIND

X	-Z	LEE SIDE DATA PLANE			CENTERLINE DATA PLANE			WINDWARD SIDE DATA PLANE		
		$\frac{U}{U_\infty}$	$\frac{V}{U_\infty}$	$\frac{W}{U_\infty}$	$\frac{U}{U_\infty}$	$\frac{V}{U_\infty}$	$\frac{W}{U_\infty}$	$\frac{U}{U_\infty}$	$\frac{V}{U_\infty}$	$\frac{W}{U_\infty}$
-750	175	-.67	.39	.041	-.66	.41	.050	-.63	.41	.018
-300	100	-.65	.36	.033	-.64	.37	.048	-.61	.41	.0015
-150	81	-.62	.35	.031	-.63	.35	.037	-.62	.42	-.0074
- 50	68	-.61	.34	.017	-.60	.34	.020	-.55	.40	-.0084
50	54	-.59	.33	.0029	-.56	.31	.012	-.51	.37	.0020
150	41	-.58	.33	.0032	-.52	.29	-.0046	-.50	.29	-.016
250	28	-.57	.33	.0002	-.49	.26	-.0028	-.45	.26	-.0081
350	15	-.53	.31	-.012	-.47	.24	-.0036	-.45	.19	-.014
512	15	-.54	.32	-.0040	-.46	.25	-.0047	-.42	.20	-.019
675	15	-.54	.34	-.0007	-.45	.25	-.011	-.40	.20	-.014
838	15	-.52	.34	-.0098	-.47	.26	-.011	-.41	.18	-.014
1000	15	-.45	.31	-.011	-.49	.29	-.0095	-.40	.20	-.015
1100	28	-.45	.30	-.014	-.53	.32	-.010	-.41	.24	-.011
1200	41	-.47	.32	-.0075	-.57	.33	-.0093	-.42	.30	-.012
1300	54				-.60	.36	-.0064	-.45	.35	-.0077
1400	68	-.53	.34	-.0029	-.63	.38	-.0081	-.48	.35	-.0077
1500	81	-.54	.34	-.0014	-.64	.38	-.010	-.52	.36	-.011
1600	94	-.57	.35	-.0022	-.62	.37	-.013	-.56	.39	.0002
1700	107	-.61	.37	.0061	-.61	.35	-.021	-.63	.41	-.0043
1875	130	-.66	.38	.0013	-.61	.34	-.023	-.70	.41	-.0050
2050	153	-.70	.39	-.028	-.72	.38	-.037	-.76	.42	-.0094
2200	174	-.72	.41	-.055	-.75	.40	-.060	-.77	.42	-.024
2350	194	-.73	.41	-.042	-.75	.42	-.057	-.76	.42	-.022
2650	233	-.74	.40	-.022	-.77	.39	-.014	-.75	.41	-.035
2950	272	-.79	.41	.004	-.77	.40	-.012	-.80	.41	-.025

TABLE 3

THREE-DIMENSIONAL TURBULENCE INTENSITIES IN PERCENT

| X(ft)	-z(ft)	WIND AT 0 DEGREES CENTERLINE DATA PLANE			WIND AT 0 DEGREES SIDE DATA PLANE			WIND AT 30 DEGREES LEE SIDE DATA PLANE			WIND AT 30 DEGREES CENTER DATA PLANE			WIND AT 30 DEGREES WINDWARD SIDE DATA PLANE		
		$\frac{u_{rms}}{U_{vector}}$ (%)	$\frac{w_{rms}}{U_{vector}}$ (%)	$\frac{v_{rms}}{U_{vector}}$ (%)	$\frac{u_{rms}}{U_{vector}}$ (%)	$\frac{w_{rms}}{U_{vector}}$ (%)	$\frac{v_{rms}}{U_{vector}}$ (%)	$\frac{u_{rms}}{U_{vector}}$ (%)	$\frac{w_{rms}}{U_{vector}}$ (%)	$\frac{v_{rms}}{U_{vector}}$ (%)	$\frac{u_{rms}}{U_{vector}}$ (%)	$\frac{w_{rms}}{U_{vector}}$ (%)	$\frac{v_{rms}}{U_{vector}}$ (%)	$\frac{u_{rms}}{U_{vector}}$ (%)	$\frac{w_{rms}}{U_{vector}}$ (%)	$\frac{v_{rms}}{U_{vector}}$ (%)
-750	175	8.2	4.5	5.6	7.4	4.4	5.6	8.6	5.2	7.0	8.2	4.1	6.3	8.9	5.2	7.6
-300	100	10.7	5.7	7.1	9.8	5.1	7.0	9.5	5.6	7.4	9.5	5.2	8.2	9.9	5.7	8.2
-150	81	10.9	6.0	7.2	9.9	5.1	6.7	9.7	5.4	7.5	11.3	5.8	7.9	11.0	6.4	8.7
-50	68	11.0	6.0	7.2	9.8	5.5	7.0	9.4	5.2	7.3	12.1	6.4	7.9	12.0	6.8	9.1
50	54	11.4	6.2	7.6	10.1	5.8	7.3	8.9	5.1	7.6	11.8	6.1	8.1	14.9	7.5	10.7
150	41	11.6	6.1	7.8	10.8	5.8	7.6	9.4	4.9	7.6	11.6	6.2	8.6	18.8	8.5	12.2
250	28	12.0	5.6	7.9	11.4	5.5	7.7	9.6	4.8	7.9	11.3	5.6	8.9	19.7	8.8	13.3
350	15	12.3	5.6	8.0	11.6	5.6	7.9	10.0	4.6	8.2	11.5	5.4	8.9	20.1	7.9	13.8
512	15	12.6	5.6	8.0	12.2	5.5	8.3	9.9	4.6	8.6	12.1	5.1	9.0	21.6	8.4	14.2
675	15	13.2	6.3	8.5	13.1	5.1	8.3	9.8	4.7	8.1	11.3	5.1	8.7	21.3	8.1	14.8
858	15	13.8	6.4	8.7	13.2	6.1	8.5	10.3	4.9	8.1	10.6	5.1	8.8	19.7	8.4	15.8
1000	15	14.7	6.8	9.4	13.8	6.5	8.8	11.8	5.3	8.6	10.6	4.7	8.4	20.6	8.2	13.7
1100	28	15.1	7.0	9.3	13.9	6.6	9.0	11.2	5.7	9.1	10.2	4.8	8.1	22.3	9.5	15.1
1200	41	15.6	7.7	9.5	14.1	6.8	8.7	11.0	6.5	10.3	9.9	5.2	8.5	15.0	8.0	10.8
1300	54	16.4	8.0	9.6	14.5	7.2	8.8	11.5	7.0	10.6	9.6	5.4	8.1	17.2	8.3	11.3
1400	68	16.7	8.1	9.9	14.7	7.2	8.7	11.9	7.0	10.6	9.5	5.2	7.7	14.6	7.7	11.1
1500	81	16.8	8.5	9.5	15.5	6.6	8.1	12.3	7.0	10.8	10.1	5.4	7.6	12.7	7.3	11.3
1600	94	15.6	7.3	8.7	12.1	6.2	7.5	11.4	6.7	10.0	11.0	5.6	7.6	10.6	6.3	9.6
1700	107	14.9	6.8	8.1	10.3	5.2	6.4	10.2	5.8	8.6	12.2	6.0	7.9	9.2	5.0	6.8
1875	130	11.0	5.8	6.7	9.0	4.7	6.3	9.2	5.1	7.3	10.0	6.0	8.7	7.9	4.6	6.5
2050	155	7.6	4.6	5.3	6.6	3.8	4.9	6.3	4.1	5.5	5.7	3.6	5.5	6.3	4.3	5.8
2200	174	6.0	3.7	4.7	5.4	3.7	4.4	4.3	2.9	4.4	5.0	3.6	4.8	5.4	4.0	5.0
2350	194	4.2	2.9	3.1	5.0	3.6	4.1	4.5	3.2	4.6	4.9	3.5	4.6	6.0	4.0	4.8
2650	233	4.9	3.3	3.9	5.2	3.9	4.3	4.6	3.3	4.4	5.0	3.4	4.0	5.1	3.7	4.7
2950	272													4.9	3.7	4.6
3550	350													3.2	3.0	3.1

Figure 1. Plan View of Environmental Wind Tunnel
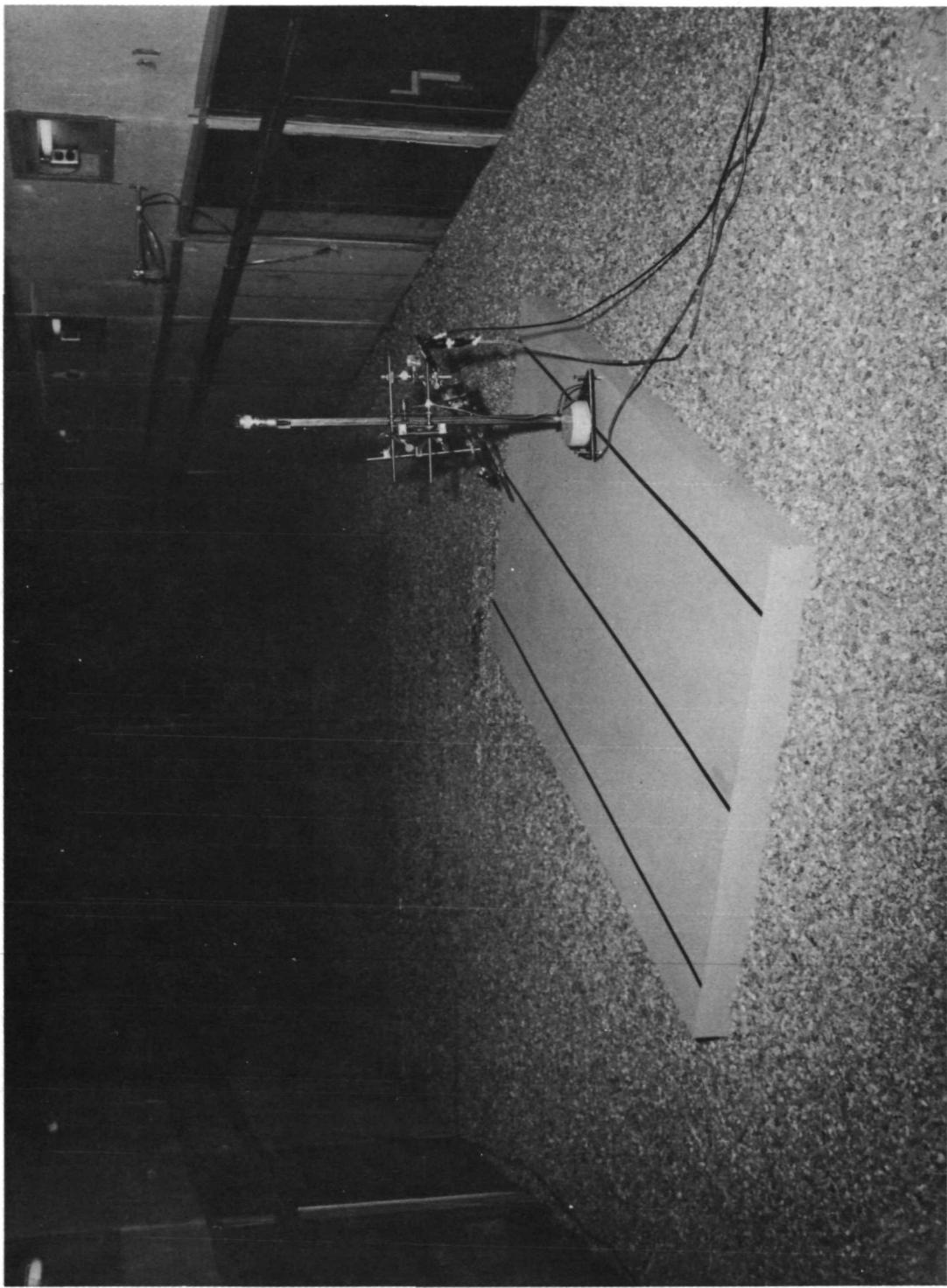
Figure 2. Model installed in the wind tunnel for 30 degree wind.

Figure 3.　Hot Wire probe.
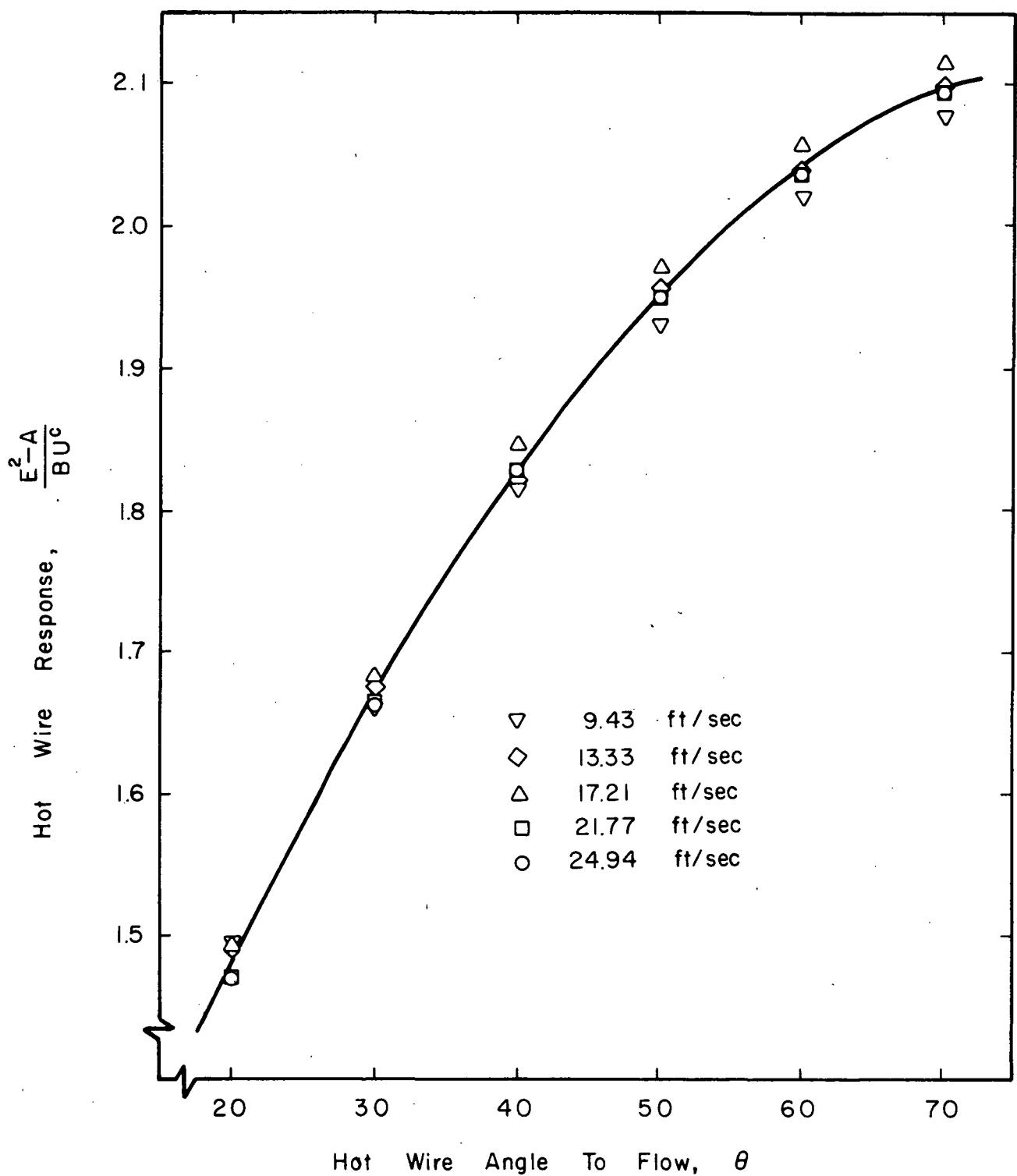
Figure 4. Typical hot-wire calibration
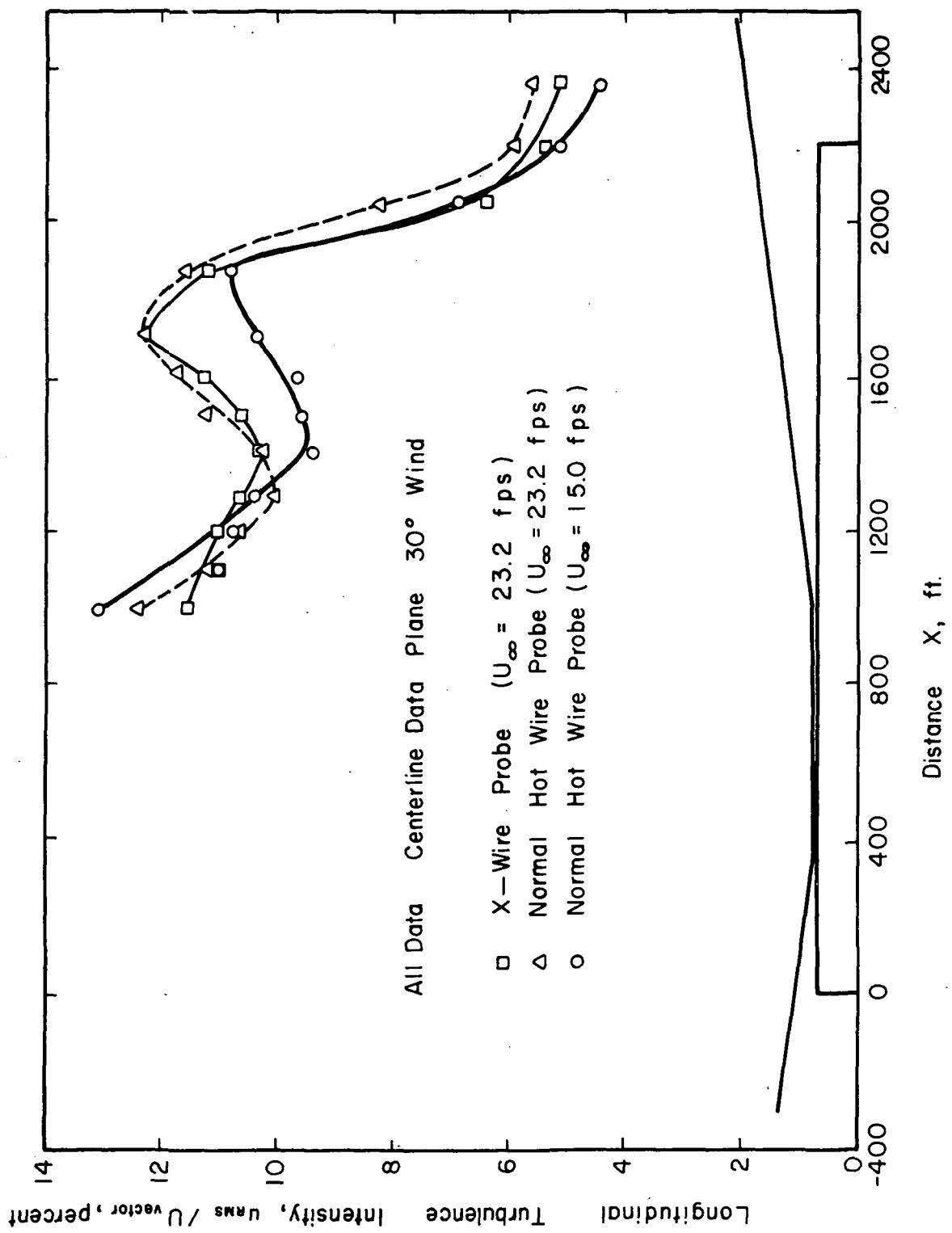
Figure 5. Results of hot-wire anemometer turbulence validation tests
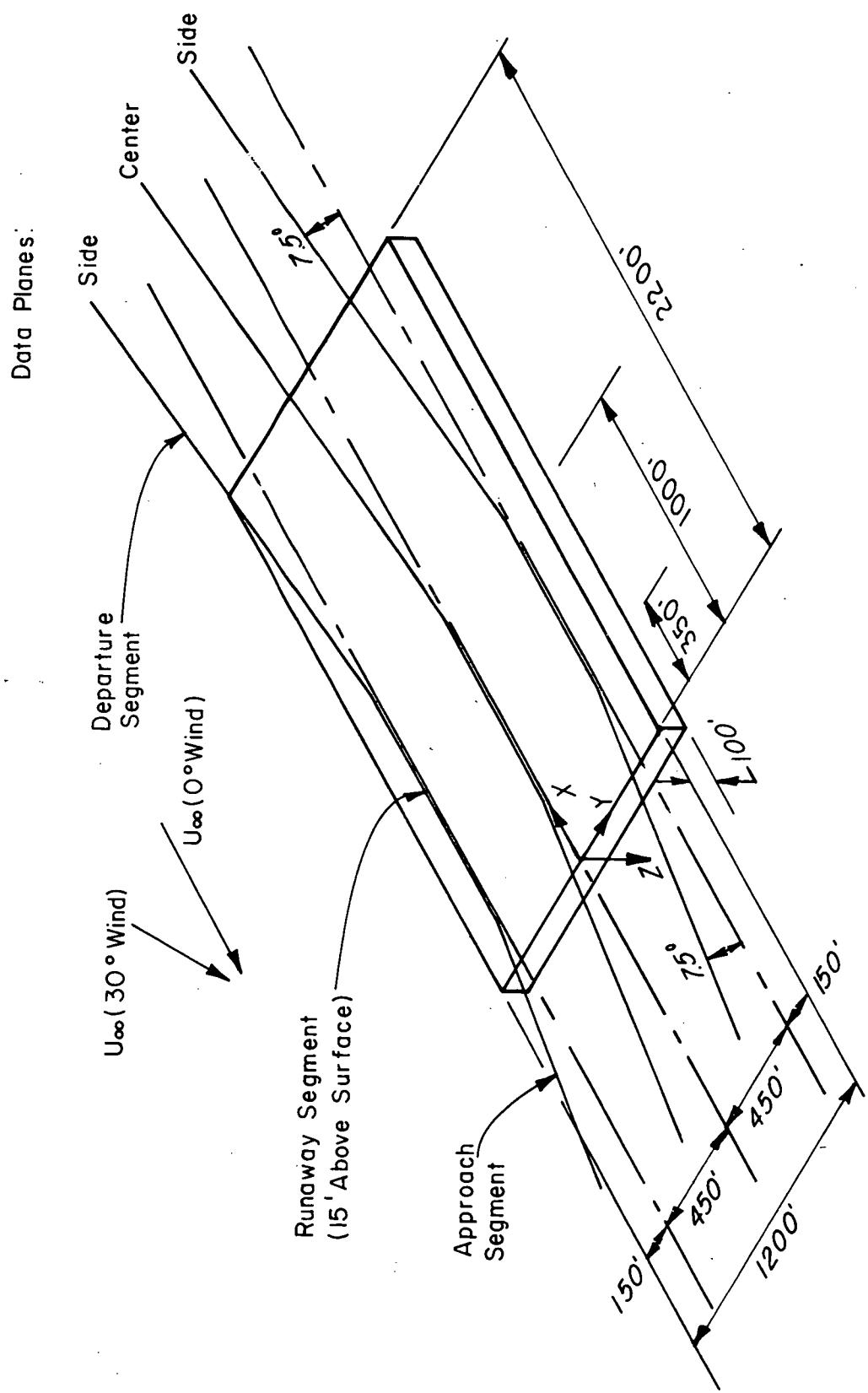
Figure 6. Data lines and coordinate system
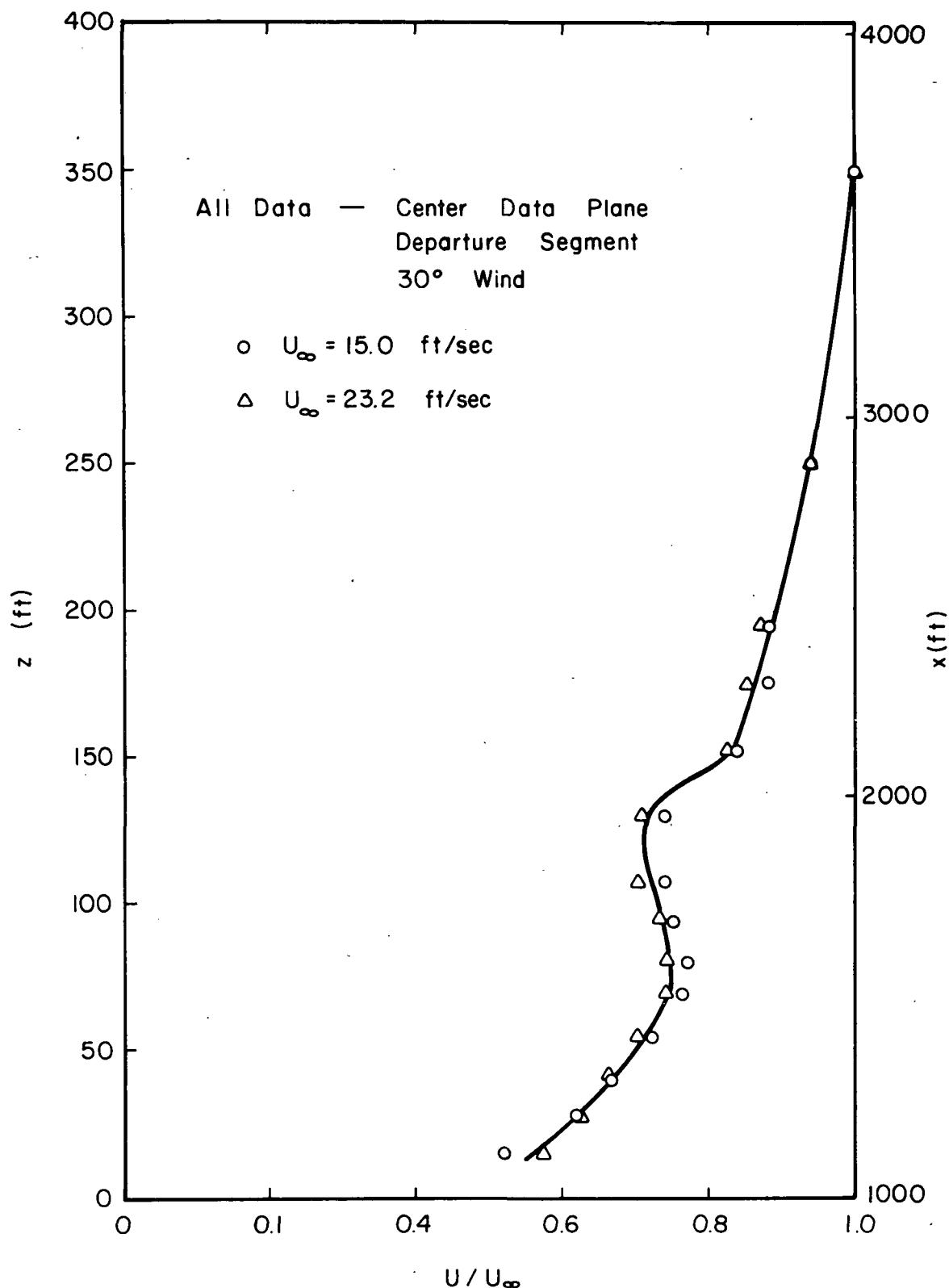
Figure 7. Demonstration of Reynolds number independence for velocity

28
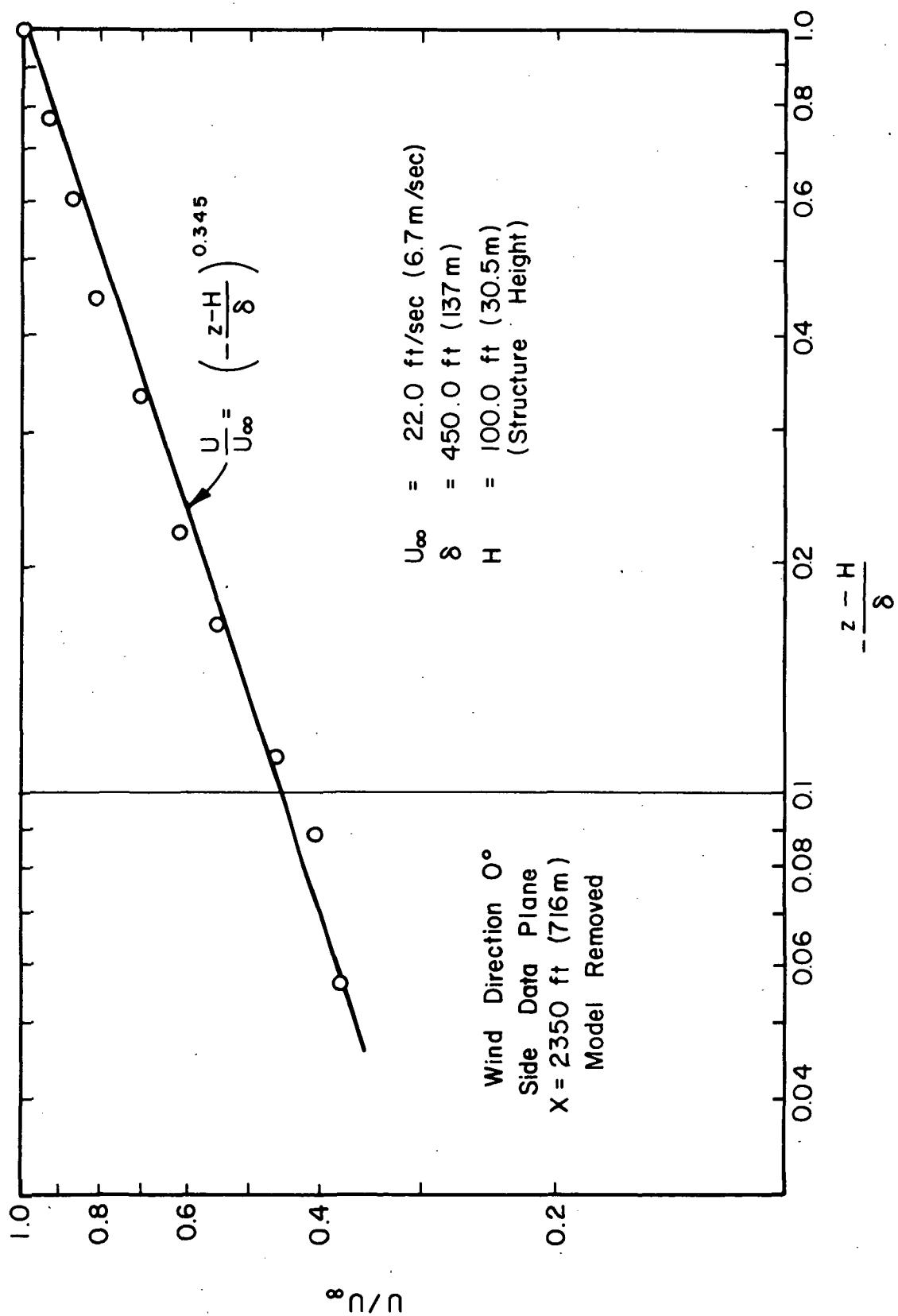


Figure 8. Mean velocity profile in logarithmic form
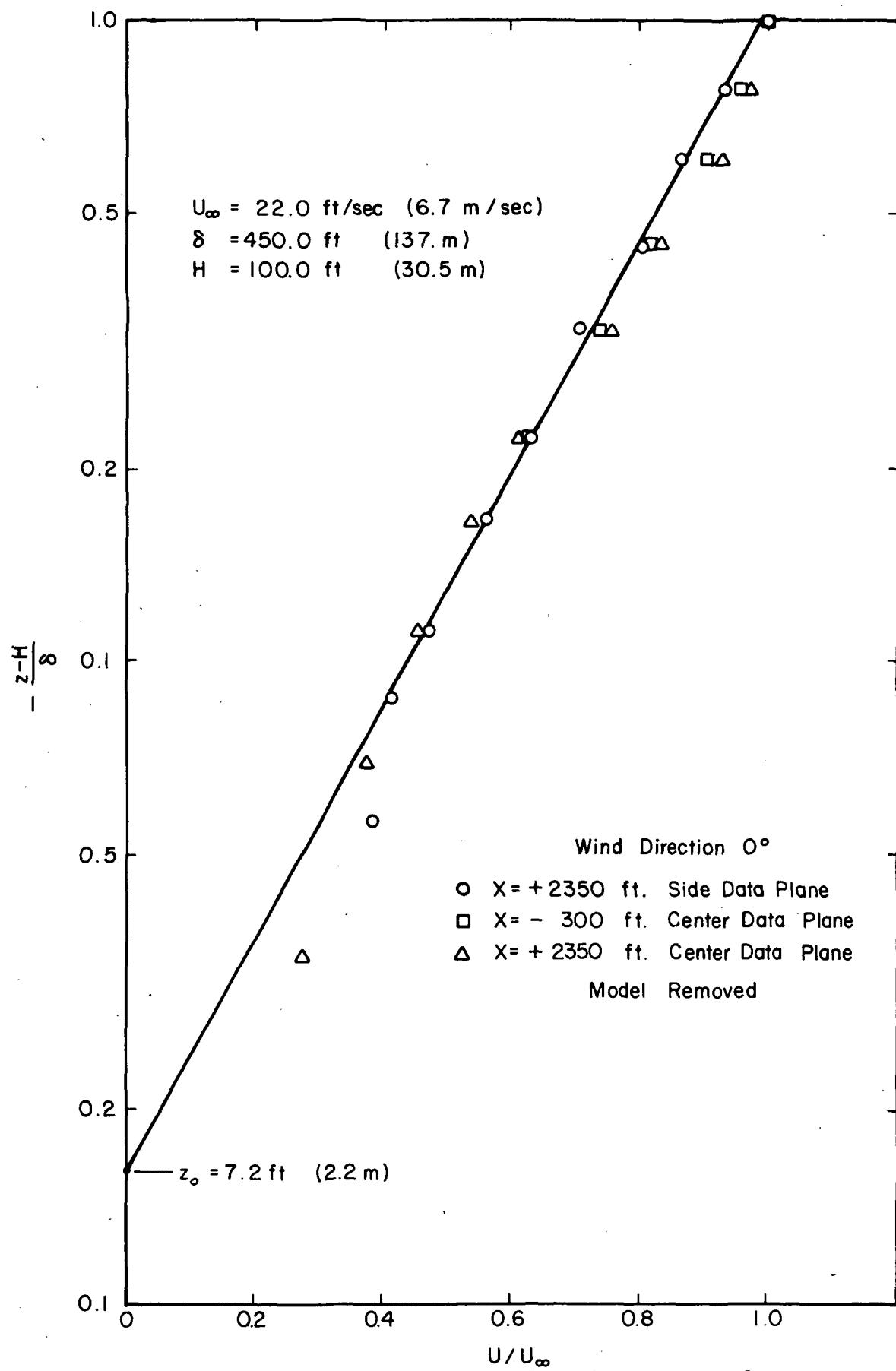
Figure 9. Mean velocity profile in semi-logarithmic form
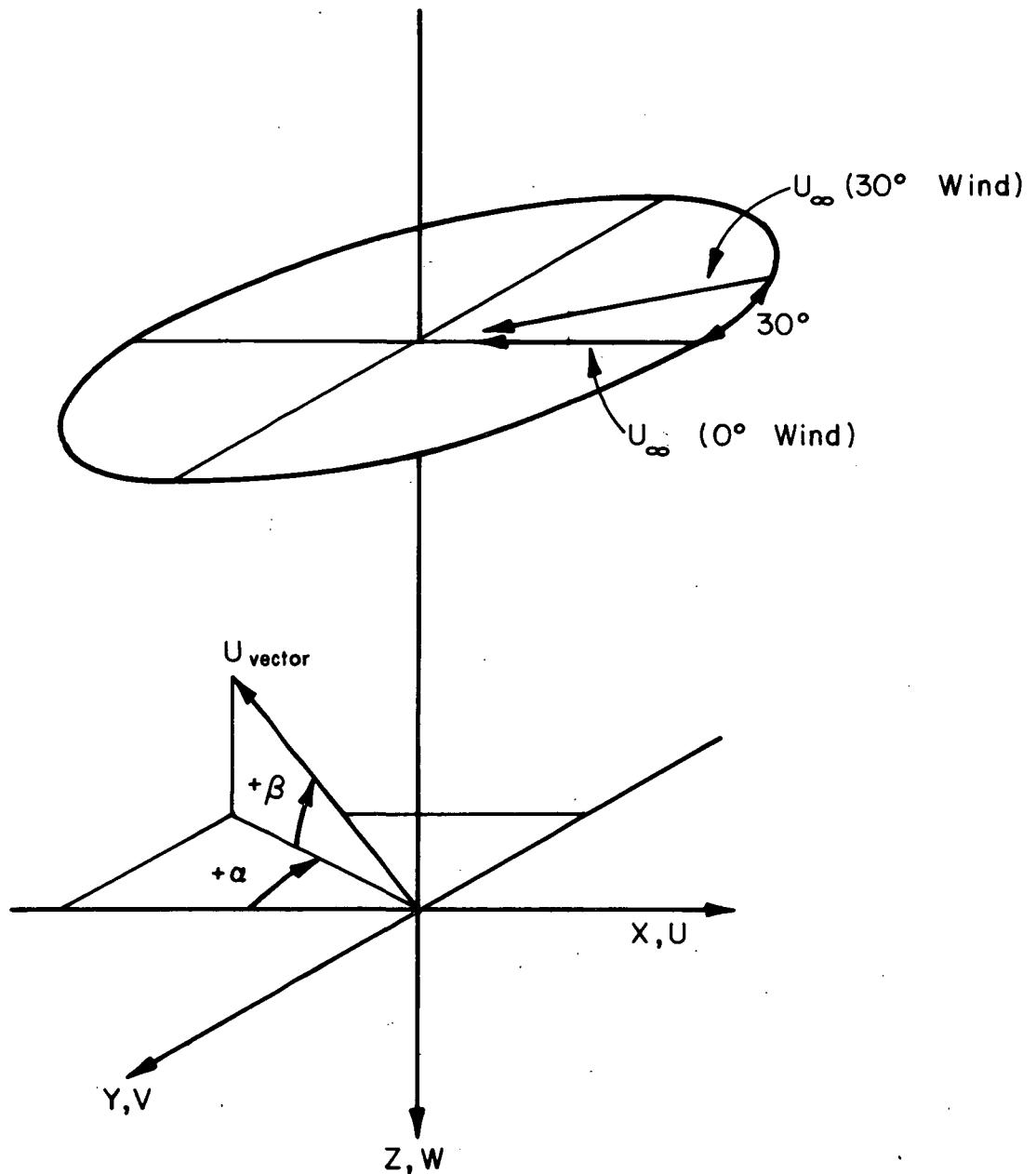
Figure 10. Definitions of angles α and β
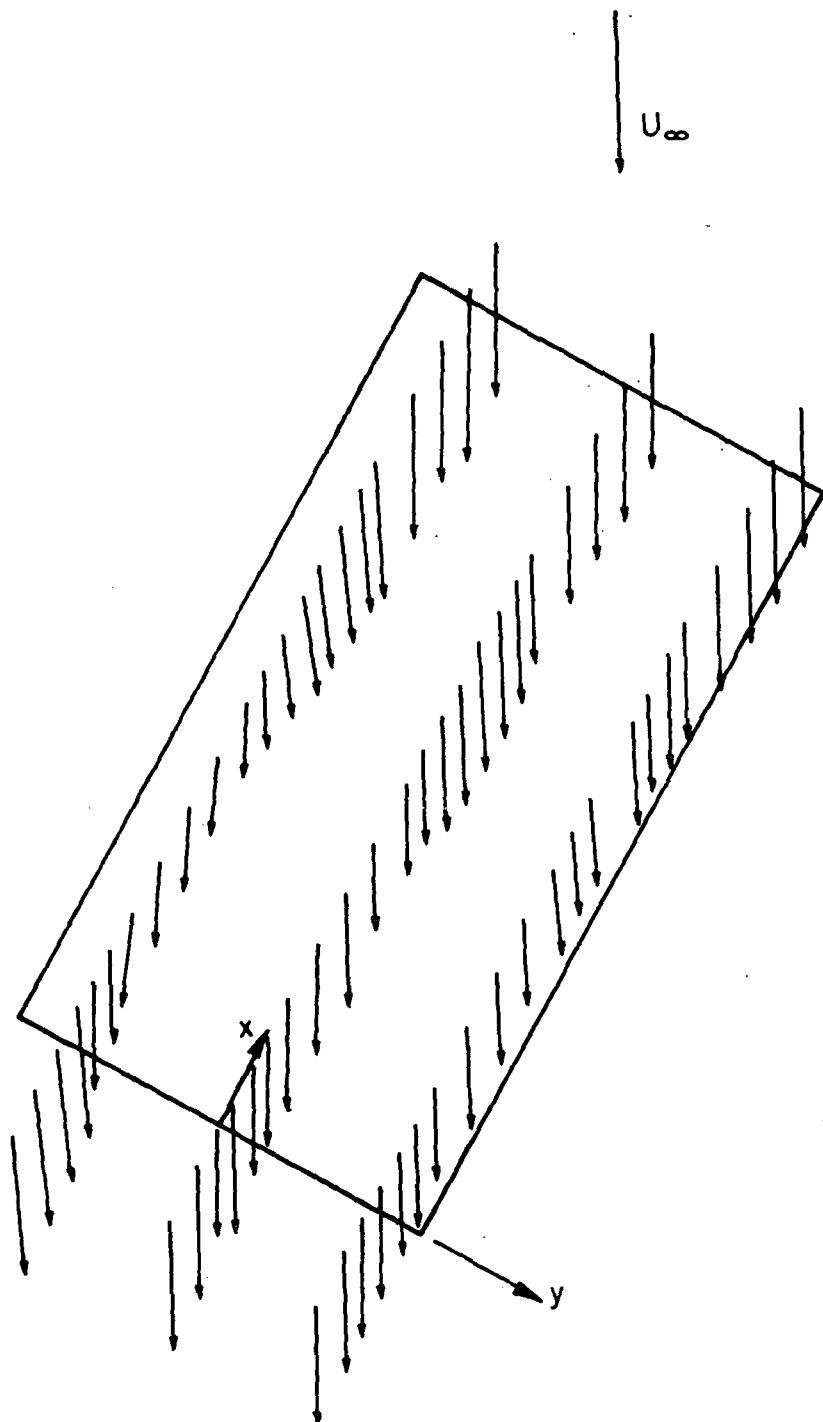
Figure 11. Mean flow magnitude and direction for 30 degree wind
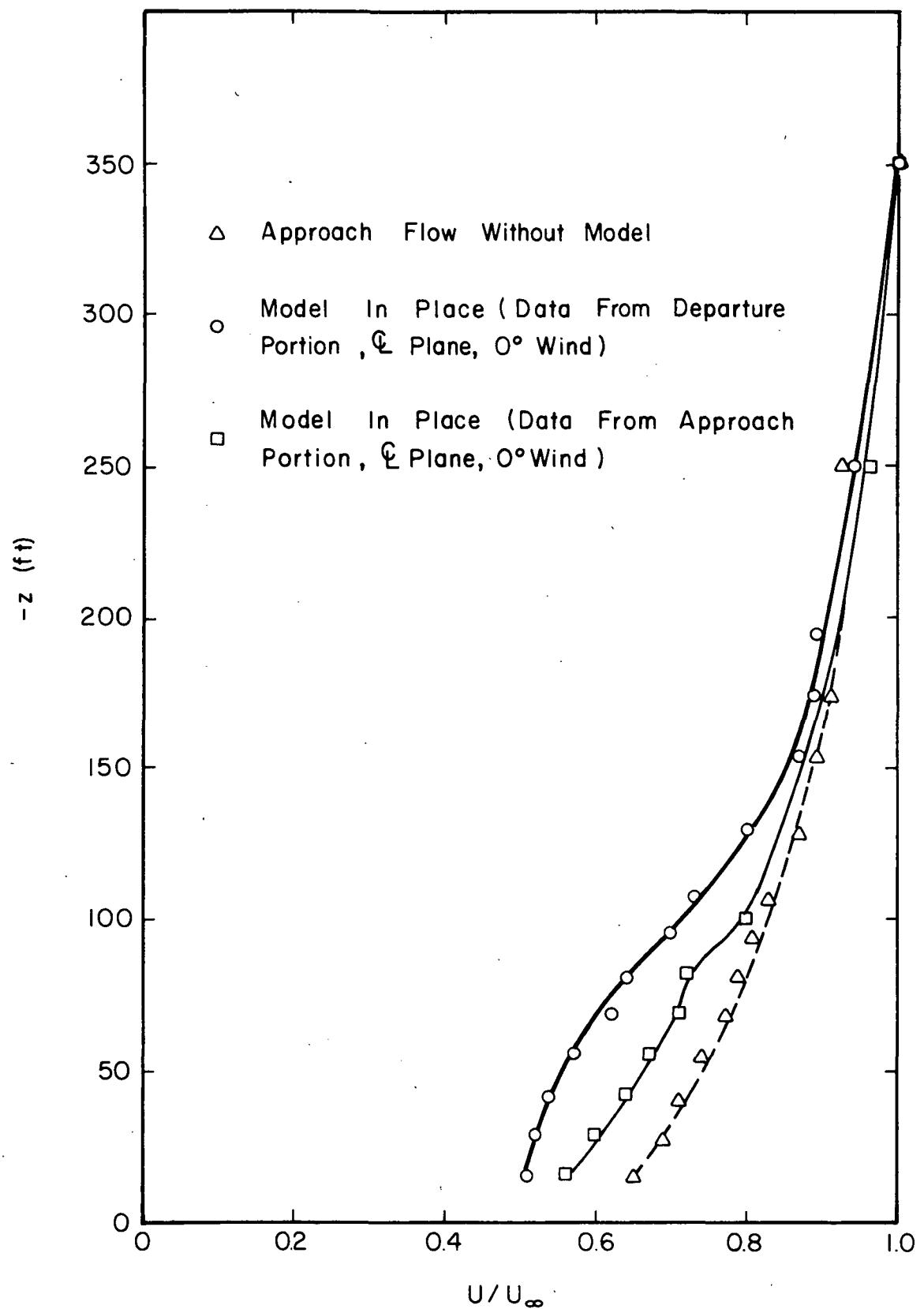
Figure 12. Mean velocity with and without model in place
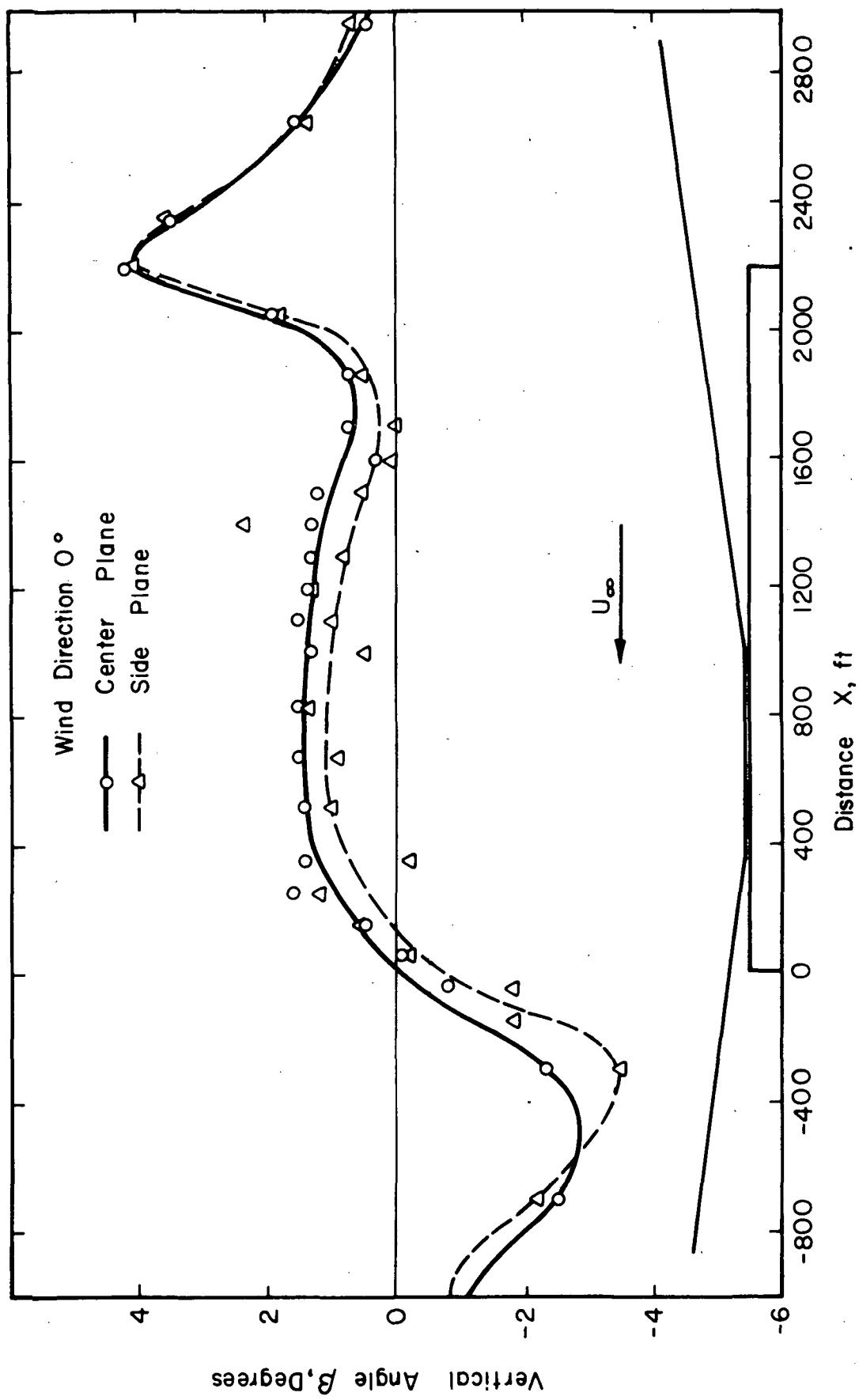
Figure 13. Vertical flow angles for 0 degree wind
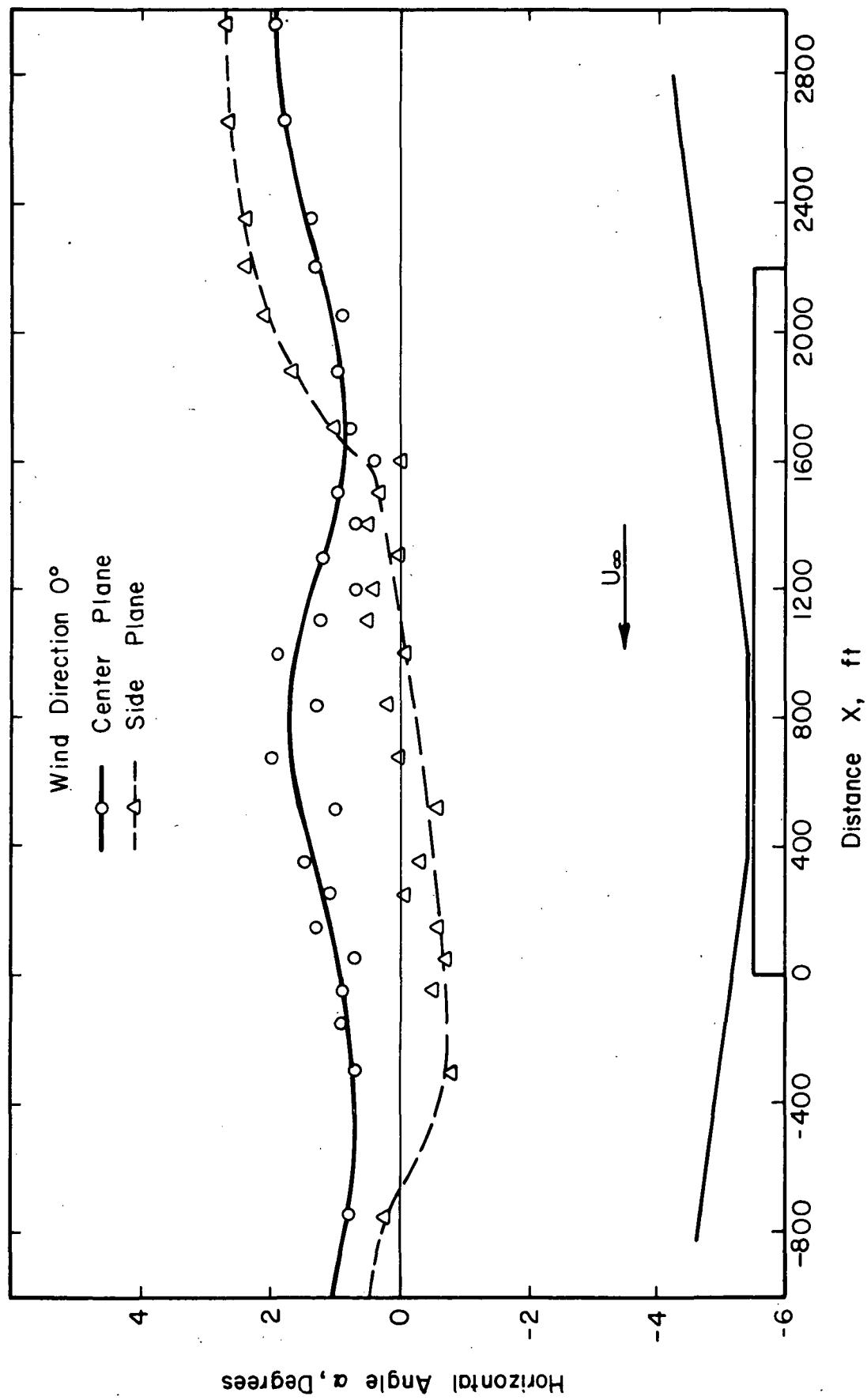
Figure 14. Horizontal flow angles for 0 degree wind
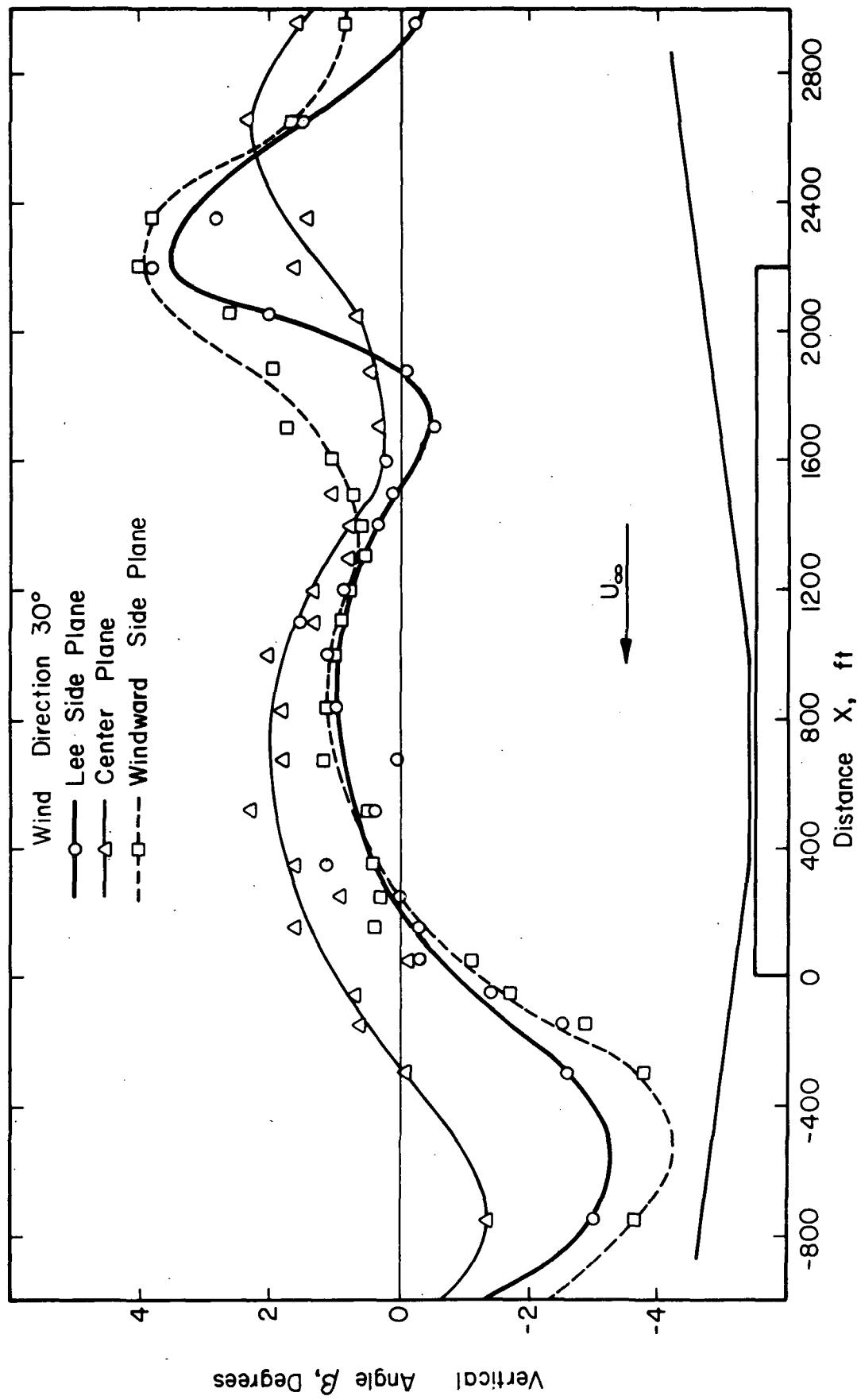
Figure 15. Vertical flow angles for 30 degree wind
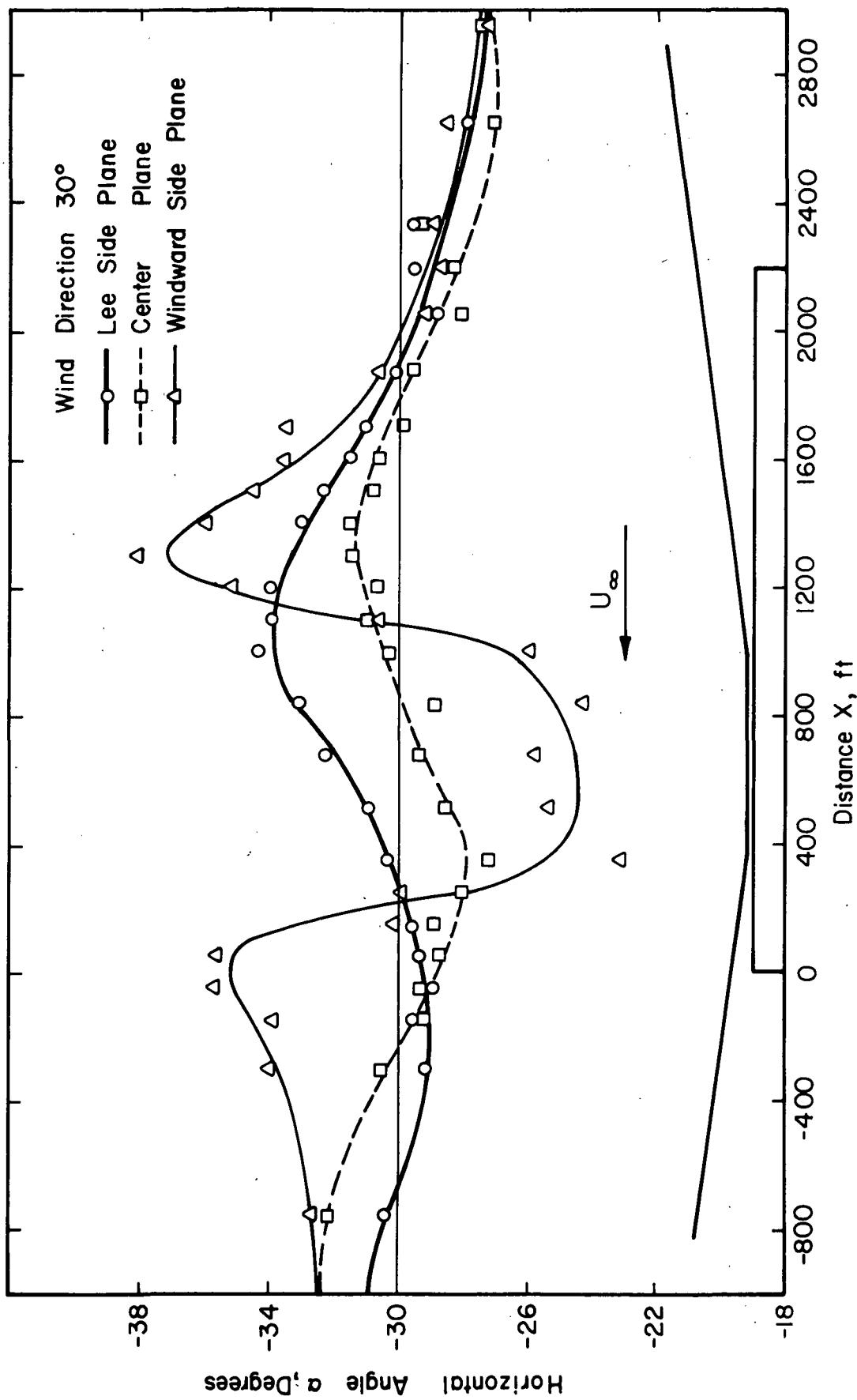
Figure 16. Horizontal flow angles for 30 degree wind
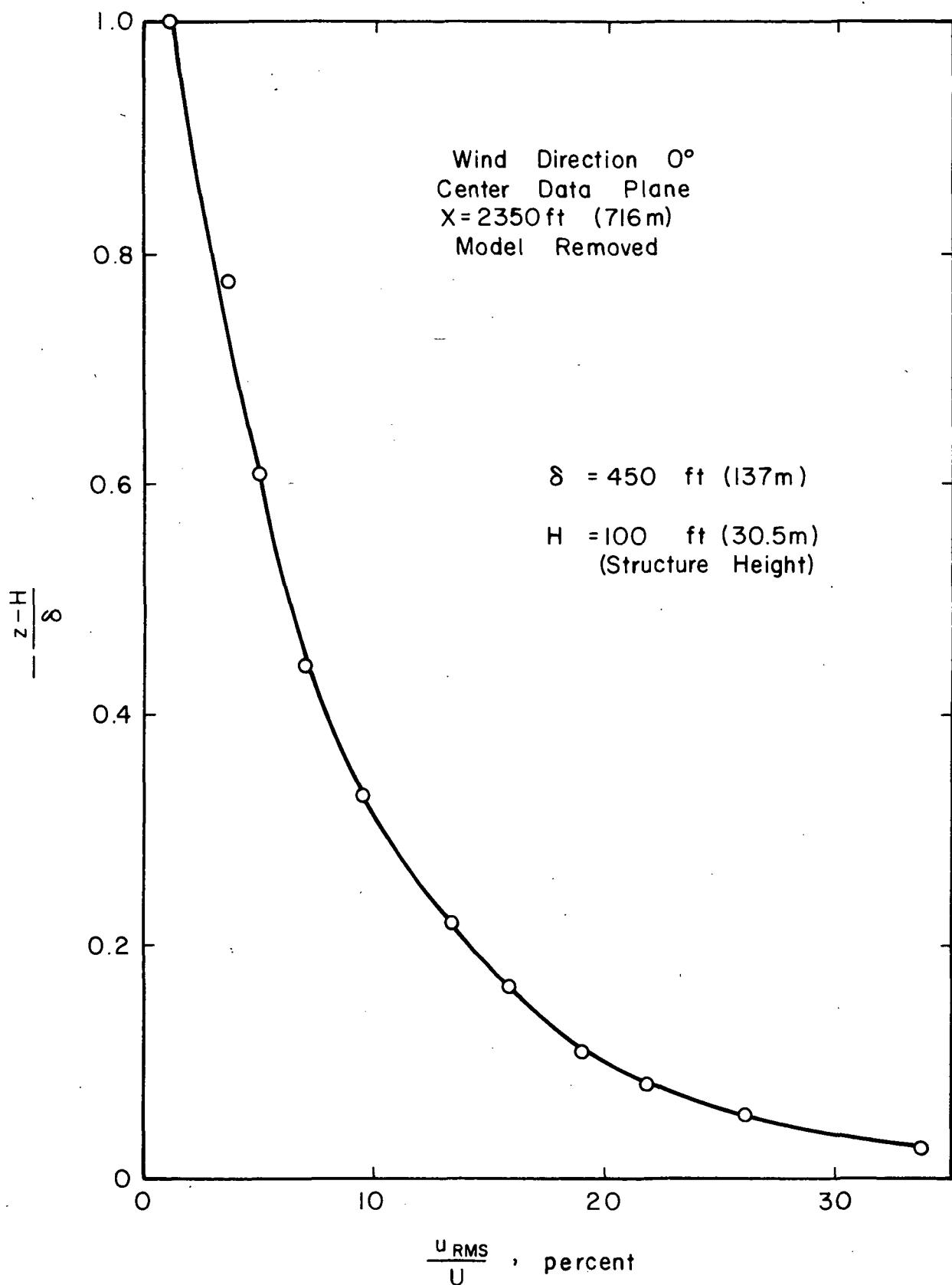
Figure 17.   Longitudinal turbulence intensity without model
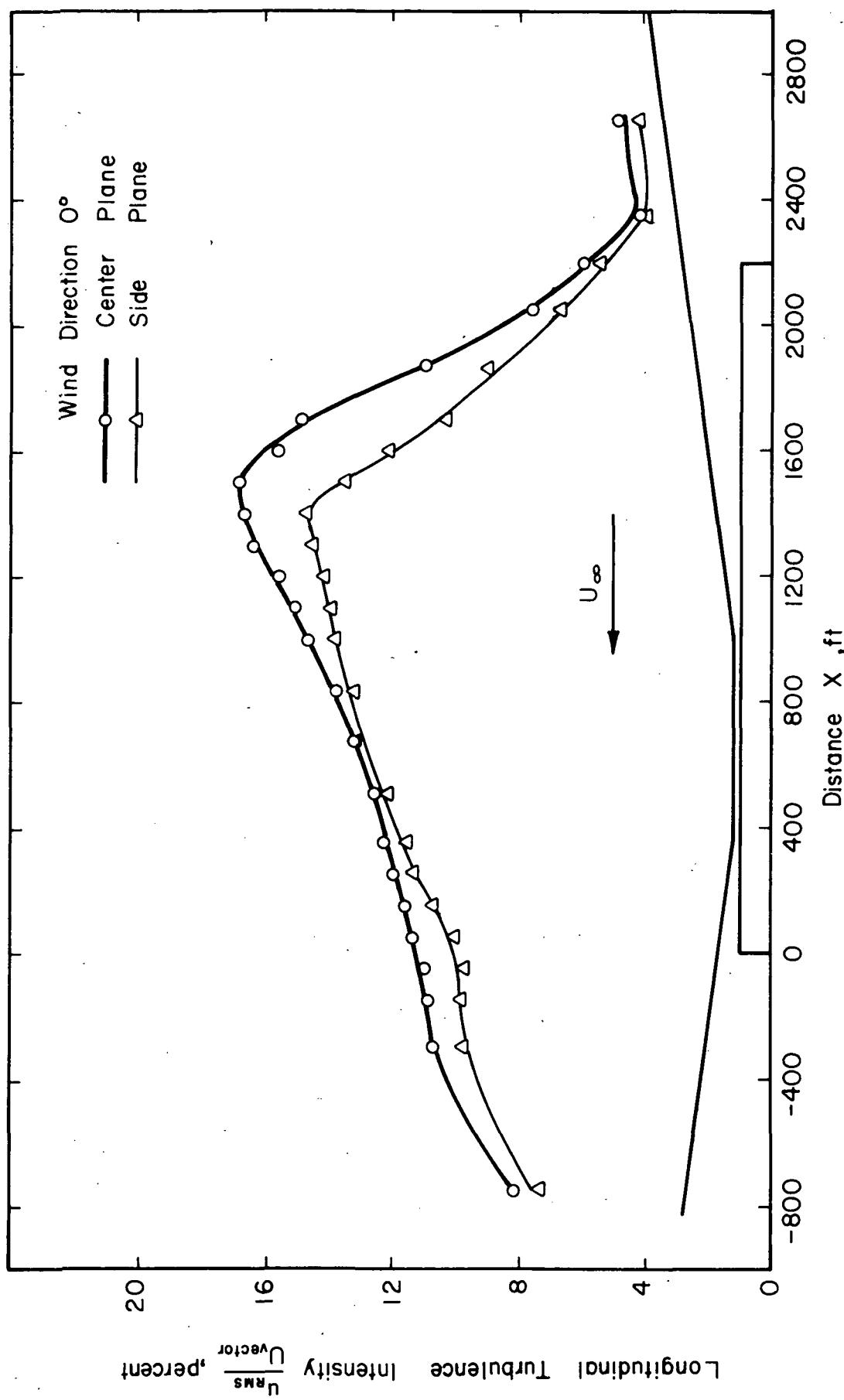
Figure 18. Longitudinal turbulence intensity for 0 degree wind
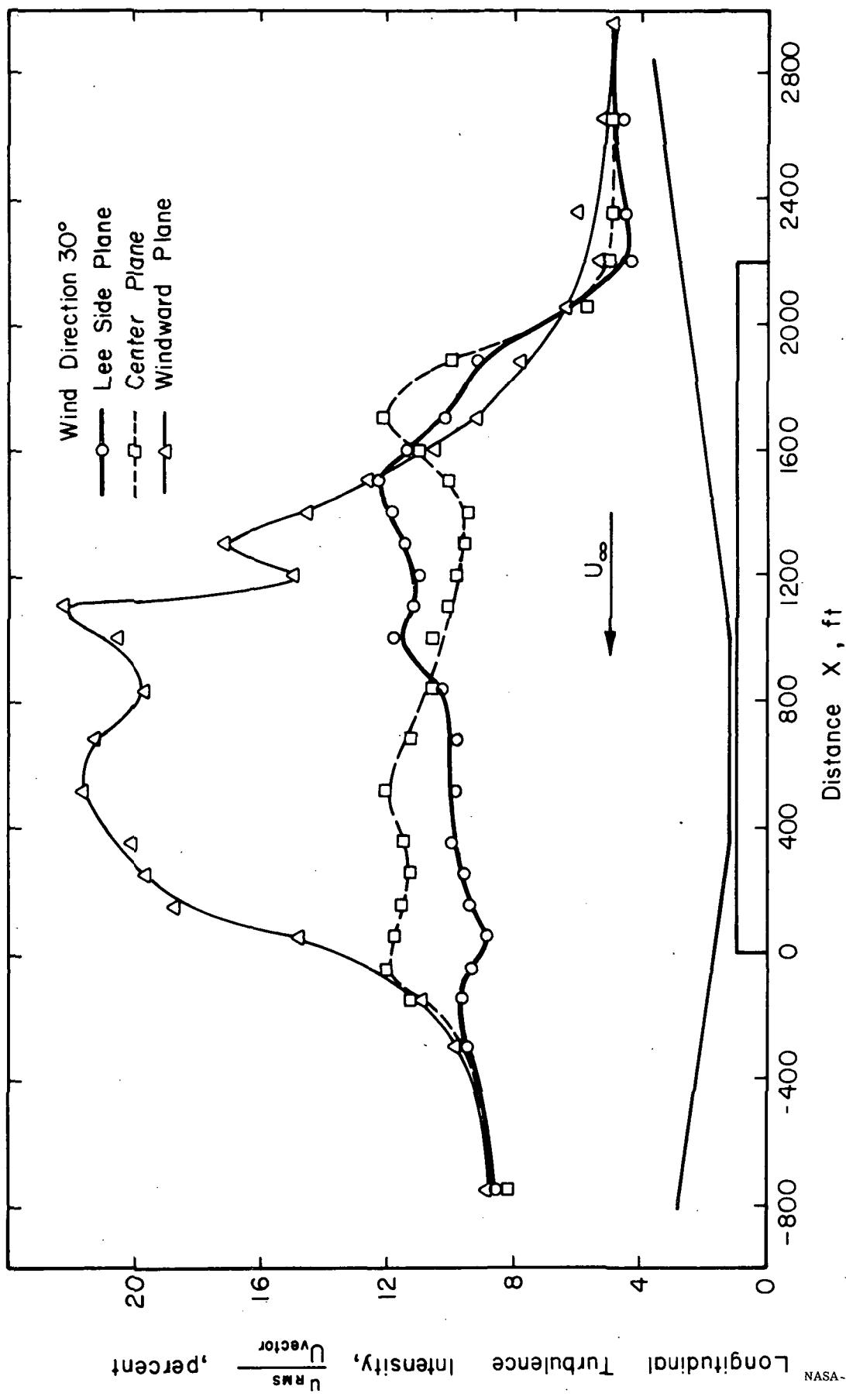
Figure 19. Longitudinal turbulence intensity for 30 degree wind

"The aeronautical and space activities of the United States shall be conducted so as to contribute . . . to the expansion of human knowledge of phenomena in the atmosphere and space. The Administration shall provide for the widest practicable and appropriate dissemination of information concerning its activities and the results thereof."
—NATIONAL AERONAUTICS AND SPACE ACT OF 1958

NASA SCIENTIFIC AND TECHNICAL PUBLICATIONS

TECHNICAL REPORTS: Scientific and technical information considered important, complete, and a lasting contribution to existing knowledge.

TECHNICAL NOTES: Information less broad in scope but nevertheless of importance as a contribution to existing knowledge.

TECHNICAL MEMORANDUMS: Information receiving limited distribution because of preliminary data, security classification, or other reasons. Also includes conference proceedings with either limited or unlimited distribution.

CONTRACTOR REPORTS: Scientific and technical information generated under a NASA contract or grant and considered an important contribution to existing knowledge.

TECHNICAL TRANSLATIONS: Information published in a foreign language considered to merit NASA distribution in English.

SPECIAL PUBLICATIONS: Information derived from or of value to NASA activities. Publications include final reports of major projects, monographs, data compilations, handbooks, sourcebooks, and special bibliographies.

TECHNOLOGY UTILIZATION PUBLICATIONS: Information on technology used by NASA that may be of particular interest in commercial and other non-aerospace applications. Publications include Tech Briefs, Technology Utilization Reports and Technology Surveys.

Details on the availability of these publications may be obtained from:

SCIENTIFIC AND TECHNICAL INFORMATION OFFICE

NATIONAL AERONAUTICS AND SPACE ADMINISTRATION
Washington, D.C. 20546